JOURNAL OF PROPULSION AND POWER
Vol. 19, No. 4, July–August 2003

Measurements and Simulation of Orifice Flow for Micropropulsion Testing

A. A. Alexeenko,* S. F. Gimelshein,† and D. A. Levin‡
Pennsylvania State University, University Park, Pennsylvania 16802
A. D. Ketsdever§
U.S. Air Force Research Laboratory, Edwards Air Force Base, California 93524
and
M. S. Ivanov¶
Institute of Theoretical and Applied Mechanics, 630090, Novosibirsk, Russia

Numerical and experimental results for a rarefied gas expansion through a thin circular orifice are presented. The orifice flow was used as a calibration test for a torsional thrust stand designed to measure force levels from 10^{-6} to 10^{-3} N. Molecular nitrogen, argon, and helium at room temperature are used as test gases. The mass flux and thrust measurements are compared with the direct simulation Monte Carlo results for Knudsen numbers from 40 to 0.01 and plenum to facility background pressure ratios of $10^3 - 10^7$. Factors that affect the total propulsive force, such as jet backflow and facility background gas penetrating the jet, are analyzed. The measured and calculated mass flux and total propulsive force were found to agree well for Knudsen numbers less than 1.

Nomenclature

A = orifice area, m^2
d = orifice diameter, m
F = force, N
$\dot{m}$ = mass flux, kg/s
p = pressure, Pa
T = temperature, K
U = axial velocity, m/s
γ = specific heat ratio
μ = viscosity coefficient, kg/m · s
ρ = density, kg/m^3

Subscripts

b = background gas
j = jet
n = nozzle
0 = stagnation, plenum reservoir

I. Introduction

THE ability to measure extremely low thrust levels with high precision is becoming more critical as attempts are made to characterize the performance of emerging micropropulsion systems. The measurement of the thrust of microscale propulsion devices, such as cold gas and mono- and bipropellant thrusters, as well as resistojets, is a difficult task due to the very low thrust levels, on the order of milli- and micro-Newtons. For such force levels, facility vibrations and test stand drift can lead to significant measurement errors. On the other hand, the accurate modeling of such flows is often hampered by the many uncertainties in the flow and material characteristics such as the distribution of wall temperature, viscosity–temperature exponents for a specific mixture, and internal energy transfer models. In this case, the orifice flow with the comparable thrust levels can serve as a calibration test for milli- and micro-Newton thrust stands. This paper describes the modeling and experimental results of mass flux and thrust force for nitrogen, helium, and argon orifice flow at room temperature.

The steady flow of a gas through an infinitesimally thin orifice, so-called orifice flow, is a classical problem of fluid mechanics.[1] Besides the theoretical interest, there are many practical applications in space environment and vacuum technology where orifice flow is important. An extensive experimental study of orifice flow has been conducted in the past. For gas expansion through an orifice, the analytical solution is known for the limiting case of Knudsen number $Kn = \infty$, that is, a collisionless flow. The first-order corrections for the mass flux of a thin orifice were obtained by Liepmann[2] for near-zero and large Knudsen numbers. Numerical results for the mass flux in the near-free molecular regime were obtained with a first-iterate solution of the Boltzmann equation (see Ref. 3) and were found to agree with experimental data.[2] It is also known that in the continuum limit ($Kn = 0$) the mass flux through an orifice of negligible lip thickness is always less than that of a comparable smooth nozzle.[2] The discharge coefficient (i. e., the ratio of the orifice mass flux to that of an isentropic inviscid nozzle flow with the same throat area) was measured by different workers for various gases and aperture shapes at high Reynolds numbers. The specific values may be found in Ref. 4.

In the transitional regime, the Knudsen number on the order of 0.01–10, there is no analytical solution to the orifice flow, and experimental data are scarce. Nonequilibrium phenomena, such as a nonMaxwellian velocity distribution and translational–rotational nonequilibrium, are expected to be important in this regime.[5]

This paper presents the results of direct simulation Monte Carlo (DSMC) calculations of orifice flow in the transitional regime with the specific goal of the use of the calculations for comparison with mass flux and thrust force measurements.[6] The accuracy of the DSMC simulations of a gas flow depends on two major factors: first, on the accuracy of the molecular model used to represent the

Presented as Paper 2001-3072 at the 35th Thermophysics Conference, Anaheim, CA, 11–14 June 2001; received 18 July 2002; revision received 11 February 2003; accepted for publication 24 February 2003.

*Graduate Student, Aerospace Engineering Department; alexeenko@psu.edu. Student Member AIAA.
†Senior Research Scientist, Aerospace Engineering Department. Member AIAA.
‡Associate Professor, Aerospace Engineering Department; dalevin@psu.edu. Senior Member AIAA.
§Senior Research Engineer, Propulsion Directorate. Senior Member AIAA.
¶Head of Computational Aerodynamics Laboratory. Associate Fellow AIAA.

physical gas flow phenomena and second, on the accuracy of the statistical simulation itself, that is, resolution in terms of the number of simulated particles, time step, and cell size of the spatial mesh. For the experimental conditions considered in this work: room temperature, argon, nitrogen, and helium test gases, molecular collision parameters such as the viscosity–temperature exponents and molecular diameters are well known. Moreover, the computational requirements are easily met for the orifice flow in the Knudsen number regime from 0.01 to 40. This allows one to obtain very accurate numerical results by applying the DSMC method.

II. Theory

In this section, the reference formulas for mass and momentum flux related to orifice flow at zero and infinite Reynolds numbers are given.[2] The Reynolds number for orifice flow can be defined as

$$Re = \rho_0 U_0 d/\mu$$

where $U_0 = \sqrt{(\gamma RT_0)}$ is the speed of sound in the reservoir. The gas properties in the reservoir (plenum) denoted with the subscript 0 will be referred to later as plenum conditions.

For zero Reynolds number (i.e., in the collisionless limit where the mean free path in the stationary gas at the reservoir is much larger than the orifice diameter), the mass flux is

$$\dot{m} = \left(1/\sqrt{2\pi RT_0}\right)(p_0 - p_b)A \tag{1}$$

and the momentum flux is

$$F = [(p_0 - p_b)/2]A \tag{2}$$

For an inviscid one-dimensional isentropic choked flow through a smooth nozzle the mass flux is

$$\dot{m}_n = \sqrt{\gamma}[2/(\gamma+1)]^{(\gamma+1)/2(\gamma-1)}\rho_0 U_0 A \tag{3}$$

and the momentum flux is

$$F_n = 2[2/(\gamma+1)]^{1/(\gamma-1)} p_0 A \tag{4}$$

The mass flux for an orifice with a negligible lip thickness is less than that of a smooth nozzle

$$\dot{m} = C_d \dot{m}_n \tag{5}$$

where $C_d = C_d(\gamma, Re)$ is the discharge coefficient of the orifice flow. A typical value of C_d for a diatomic gas is 0.85 (Ref. 4).

III. Experiment

A. Experimental Setup

The orifice has a diameter $d = 1.0$ mm and a thickness $t = 0.015$ mm and is machined in a tantalum shim attached to an aluminum plenum. The plenum is mounted on a torsional thrust stand. A schematic of the setup is shown in Fig. 1. The measurements of the mass flux have been made at the gas inlet with an mks mass flow meter. The force measurements were made by detection of the angular deflection of the thrust stand arm due to the total torque force. The angular deflection was detected by measurment of the linear displacement by the use of a linear differential voltage transducer. The details on the thrust stand characteristics are reported in Refs. 6 and 7.

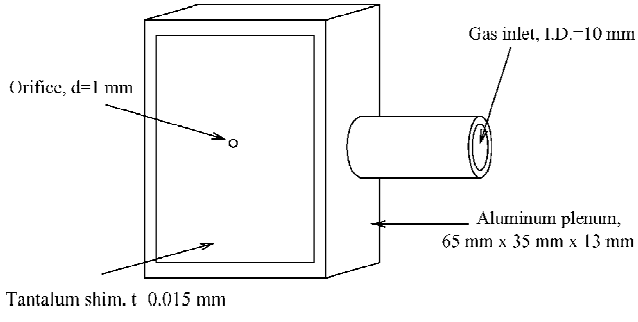

Fig. 1 Schematic of experimental geometry.

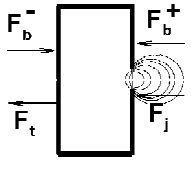

Fig. 2 Force diagram; density isolines are shown schematically.

B. Force Measurements

In ground-based low-thrust measurements, the influence of the facility background gas can be significant and has to be accounted for. The total force measured by the thrust stand is due to four sources, as shown in Fig. 2:

$$\boldsymbol{F} = \boldsymbol{F}_t + \boldsymbol{F}_j + \boldsymbol{F}_b^+ + \boldsymbol{F}_b^- \tag{6}$$

where $\boldsymbol{F}_t$ is the thrust force produced by the momentum flux through the orifice on the thrust stand, $\boldsymbol{F}_j$ is the force produced by the momentum flux of the jet gas on the surface of the plenum (jet backflow), and $\boldsymbol{F}_b^+$ and $\boldsymbol{F}_b^-$ are the forces exerted by the facility background gas on the two opposite plenum surfaces.

IV. Numerical Modeling

The SMILE code,[8] based on the DSMC method, is used to calculate orifice flow for vacuum and finite background pressure conditions. The majorant frequency scheme[9] of the DSMC method is utilized to model collisions between molecules. The intermolecular potential is assumed to be a variable hard sphere model[10] with the molecular parameters of Ref. 11. The jet and background gases are modeled as distinct species to study the influence of the facility background conditions. Because of the large pressure ratio between the plenum and the vacuum facility (from 10^3 to 10^7), accurate resolution of the background gas can only be obtained by the use of different background and jet species weights in the simulations.

Because of the symmetry of the problem, the axisymmetric version of the SMILE code has been used. The computational domain and the boundary conditions are shown in Fig. 3. The flow conditions for the three test gases are given in Tables 1–4. The gas flux corresponding to the given plenum and background pressure and room temperature ($T_0 = 300$ K) is modeled on the outer boundaries of the computational domain. The full momentum and energy accommodation model was assumed at the surface with a wall temperature 300 K. The collision cell size is chosen to be less than the local molecular mean free path. The number of collision cells was varied from 10,000 to 110,000, with 150,000–1,200,000 modeling particles, respectively, depending on the plenum pressure.

Let us now give some details on the calculation of forces used in the DSMC simulations. The impulse flux through the orifice F_t is

$$F_t = \int_A \rho \bar{u}^2 \, \mathrm{d}A$$

$$= \int_A \rho \left[\int_{-\infty}^{\infty} \int_{-\infty}^{\infty} \int_{0}^{\infty} u^2 f(u, v, w) \, \mathrm{d}u \, \mathrm{d}v \, \mathrm{d}w \right] \mathrm{d}A \tag{7}$$

where $f(u, v, w)$ is the velocity distribution function, ρ is the local gas density, and u is the axial velocity component. For an equilibrium

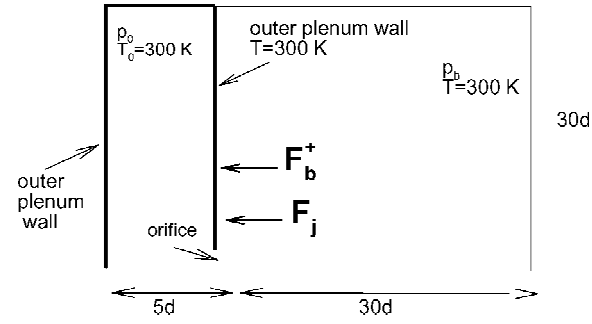

Fig. 3 Computational domain and boundary conditions.

Table 1 Reservoir and facility background conditions for nitrogen

Case	Kn	p_0, torr	p_b, torr
1	40	0.001	0
2	4	0.01	0
3	0.4	0.1	0
4	0.4	0.1	$1 \cdot 10^{-4}$
5	0.16	0.25	$1.3 \cdot 10^{-4}$
6	0.08	0.5	$1.6 \cdot 10^{-4}$
7	0.053	0.75	$1.9 \cdot 10^{-4}$
8	0.04	1.0	$2.2 \cdot 10^{-4}$
9	0.026	1.5	$2.8 \cdot 10^{-4}$
10	0.02	2.0	$3.3 \cdot 10^{-4}$
11	0.016	2.5	$3.7 \cdot 10^{-4}$
12	0.013	3.0	0
13	0.013	3.0	$2.1 \cdot 10^{-4}$
14	0.013	3.0	$4.2 \cdot 10^{-4}$
15	0.013	3.0	$6.3 \cdot 10^{-4}$
16	0.011	3.5	$4.7 \cdot 10^{-4}$

Table 2 Calculated forces for nitrogen

Case	F_t, μN	F_j, μN	F_b^-, μN	F_b^+, μN
4	6.2	0.089	1.8	1.82
5	19.2	0.661	16.5	16.9
6	42.9	1.71	19.8	20.8
7	72.4	2.90	23.3	24.7
8	99.0	4.41	26.0	28.5
9	164	7.42	31.9	36.3
10	214	9.70	36.4	42.8
11	274	12.8	39.5	48.0
14	321	17.6	44.0	54.5

Table 3 Conditions and calculated force for argon

Case	p_0, torr	$p_b \times 10^5$, torr	F, μN
17	0.077	0.72	0.45
18	0.215	1.2	1.54
19	0.686	3.0	6.24
20	1.48	6.3	14.9
21	2.00	8.1	21.6
22	2.52	9.7	28.0
23	3.06	13	34.2

Table 4 Conditions and calculated force for helium

Case	p_0, torr	$p_b \times 10^5$, torr	F, μN
24	0.868	1.0	6.50
25	1.340	1.4	11.3
26	1.816	1.8	16.8
27	2.345	2.2	22.5

velocity distribution,[11]

$$F_t = \int_A \frac{\rho RT}{2\pi^{\frac{1}{2}}} \left[s e^{-s^2} + \pi^{\frac{1}{2}} \{1 + \mathrm{erf}(s)\} \left(\frac{1}{2} + s^2 \right) \right] \mathrm{d}A \qquad (8)$$

where s is the molecular speed ratio. Equation (8) reduces to Eq. (2) for a stationary gas, $s = 0$. In the transitional flow regime, the velocity distribution function at the orifice plane is nonMaxwellian. The calculated distribution functions for the axial component of velocity at the orifice plane are plotted in Fig. 4. The distribution function changes from the half-Maxwell to the local Maxwell distribution when the Knudsen number decreases from 4 ($p_0 = 0.01$ torr) to 0.04 ($p_0 = 1$ torr). Therefore, in the transitional regime one needs to use the DSMC simulations to calculate the thrust force given by Eq. (7).

The momentum fluxes on the surface of the plenum F_j, F_b^+, and F_b^- are calculated from the pressure distribution over the corresponding surface as

$$F_j = \int_{A^+} p_1 \, \mathrm{d}A \qquad (9)$$

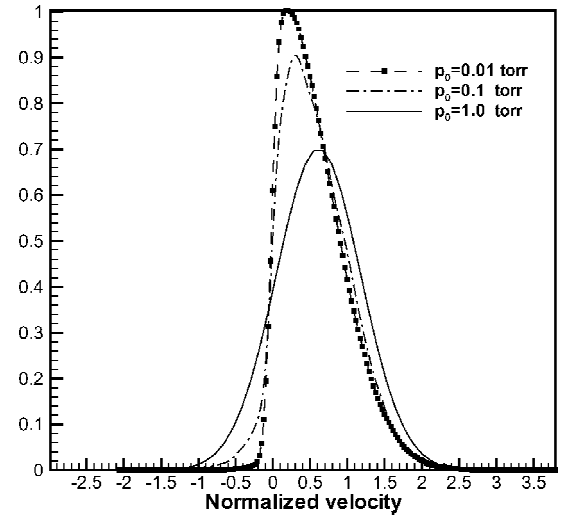

Fig. 4 Distribution function of axial velocity component at the center of the orifice.

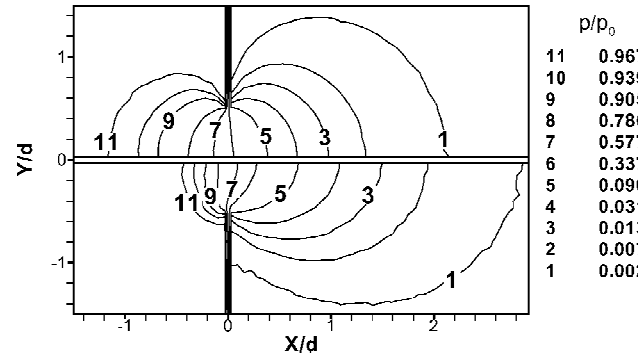

Fig. 5 Normalized pressure for $Kn = 40$ (top) and 0.01 (bottom).

$$F_b^+ = \int_{A^+} p_2 \, \mathrm{d}A \qquad (10)$$

$$F_b^- = p_b A^- \qquad (11)$$

where p_1 and p_2 are the pressure distributions on the outer plenum surface containing the orifice (see Fig. 3) for the jet and background gases, respectively, and p_b is the constant background pressure in the vacuum facility far from the orifice. The pressure distributions, p_1 and p_2, may be computed separately because the jet and background gas are treated as two distinct species. Initially, the background gas corresponds to that of a uniform background gas at p_b and $F_b^- = F_b^+$. When flow is initiated through the orifice, the background gas is perturbed and eventually is prevented from approaching the outer surface of the plenum near the orifice, a process we will refer to as jet shadowing.

V. Results and Discussion

A. Orifice Flow at Different Regimes

Note the impact of the flow rarefaction on the structure of the flow in the vicinity of the orifice. The results presented in this section are for molecular nitrogen flow at two Knudsen numbers, $Kn = 0.01$ and 40, and zero background pressure (cases 1 and 12 in Table 1). For the plenum pressure of 3 torr, the variation in background pressure from 0 to 6.3×10^{-4} torr for the plenum pressure of 3 torr does not change the flow parameters near the orifice, where the density of the jet is several orders of magnitude higher than that of the background gas.

The pressure contours normalized by the plenum pressure are shown in Fig. 5 for cases 1 and 12. The flow in the vicinity of the orifice is shown here to illustrate the impact of flow rarefaction, whereas the entire computational domain was $(-5d, 30d)$ in the

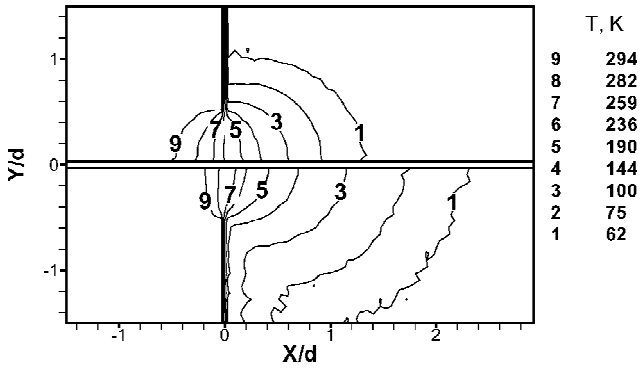

Fig. 6 Translational temperature for $Kn = 40$ (top) and 0.01 (bottom).

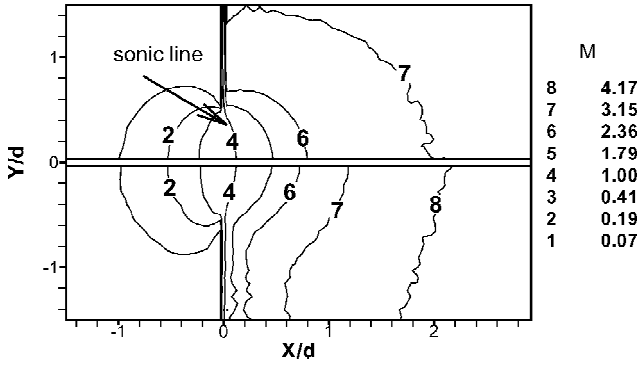

Fig. 7 Mach number for $Kn = 40$ (top) and 0.01 (bottom).

axial direction and $(0, 30d)$ in the radial direction (Fig. 3). As expected, the pressure decays more rapidly, and the influence of the orifice is observed further upstream for the more rarefied flow due to a larger mean free path. The normalized pressure at the orifice plane is about two times lower for the $Kn = 40$ case. Also, the normalized pressure for $Kn = 40$ is about two times lower than for $Kn = 0.01$ along the axis.

The flow structure for the two Knudsen numbers is different near the outer plenum wall. There are almost no collisions of jet molecules with the wall for $Kn = 40$, which is actually a free molecular flow. Pressure isolines have, therefore, a near-circular shape and start at the orifice edge for $Kn = 40$. Molecular collisions in the jet for the higher pressure case cause a backflow, with some jet molecules colliding with the outer wall and then reflecting with complete energy accommodation. This results in a gradual decrease of the pressure in the direction from the orifice edge.

The impact of the wall temperature is illustrated in Fig. 6 where the translational temperature contours are shown. For $Kn = 40$ case, the temperature isolines are normal to the plenum wall, whereas in the more dense case, $Kn = 0.01$, a large temperature gradient occurs at the wall with the gas temperature rising due to gas–surface collisions. Similar to the pressure contours, the influence of the orifice propagates further downstream for $Kn = 0.01$.

In contrast to pressure and temperature fields, the Mach number contours are similar in the subsonic portion of the flow for the two flow regimes. The Mach number contours presented for the two Knudsen numbers in Fig. 7 show that the Mach number fields weakly depend on the Knudsen number in the vicinity of the orifice (up to $M \sim 2$). The sonic line in both cases is located outside the plenum, whereas the flow at the orifice plane is subsonic in both cases.

A quantitative comparison of flow parameters across the orifice is given in Figs. 8 and 9, where the profiles of the number densities and velocities in the axial direction are shown. In Figs. 8 and 9, $Y/d = 0$ corresponds to the orifice center. The profiles were taken along the cells located immediately after the orifice plane. For $Kn = 40$, the parameters are nearly constant up to a distance of 0.4 d from the axis. In the interval from 0.4 d to the orifice edge 0.5 d, the velocity increases, and the density decreases due to the

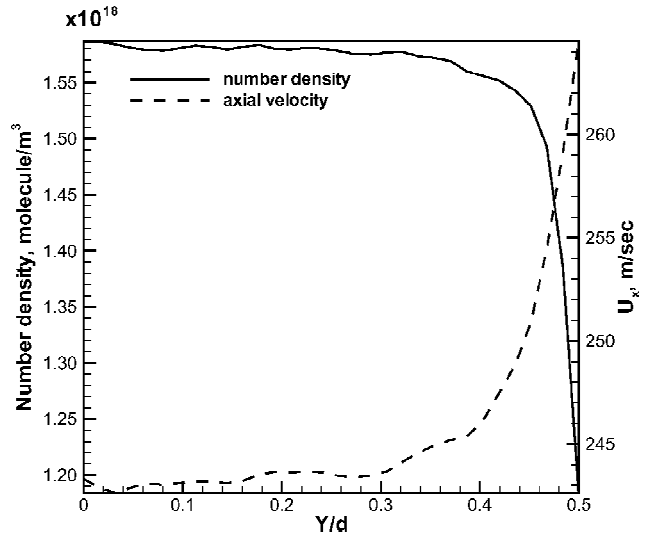

Fig. 8 Density and velocity profiles at the orifice plane for $Kn = 40$.

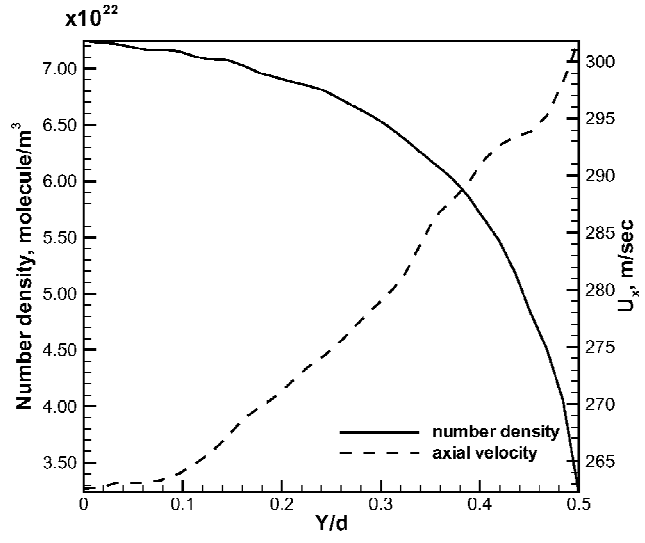

Fig. 9 Density and velocity profiles at the orifice plane for $Kn = 0.01$.

gas expansion. The shape of the density and velocity profiles are different for $Kn = 0.01$, where they more gradually change from the axis to the orifice edge.

B. Comparison of Calculated and Measured Mass Flux

A comparison of the calculated and measured mass flux is given in Fig. 10 for the nitrogen test gas cases listed in Table 1. The theoretical values of the mass flux for a free molecular flow [see Eq. (1)] and an inviscid continuum flow through an orifice with a negligible lip thickness [see Eq. (5)] are also shown here. A discharge coefficient of 0.86 for the continuum flow obtained in previous work[6] is used here. The calculated mass flux for the two lowest pressure values ($Kn = 40$ and 4) are nearly identical to the free molecular value. Calculated mass flux approaches the continuum values as the pressure is increased. The agreement between the calculated and measured mass fluxes for pressures higher than 0.5 torr is within 2%. The agreement is worse for the lowest pressures values because of greater experimental errors of approximately 14% for $p_0 = 0.1$ torr and 3.5% for $p_0 = 0.25$ torr. The comparison of calculated and measured mass fluxes for argon is given in Fig. 11. The similar agreement was obtained for the helium gases.

C. Effect of the Jet on the Background Gas

Consider now the effect of the jet on the flowfields and surface fluxes of the background gas. As expected, the jet molecules do

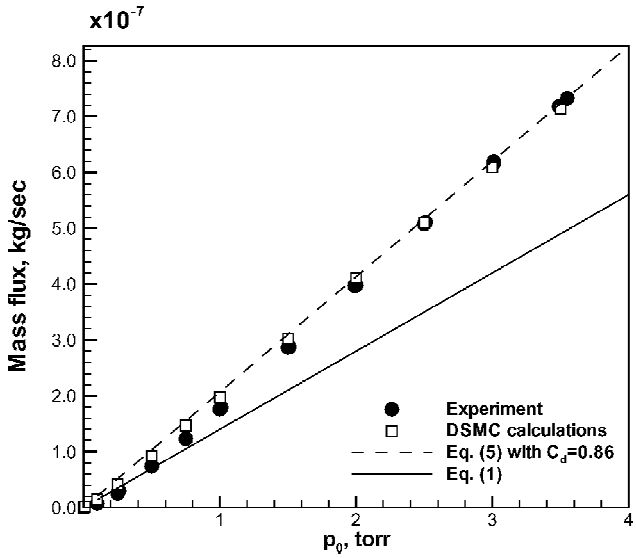

Fig. 10 Mass flux vs plenum pressure for nitrogen.

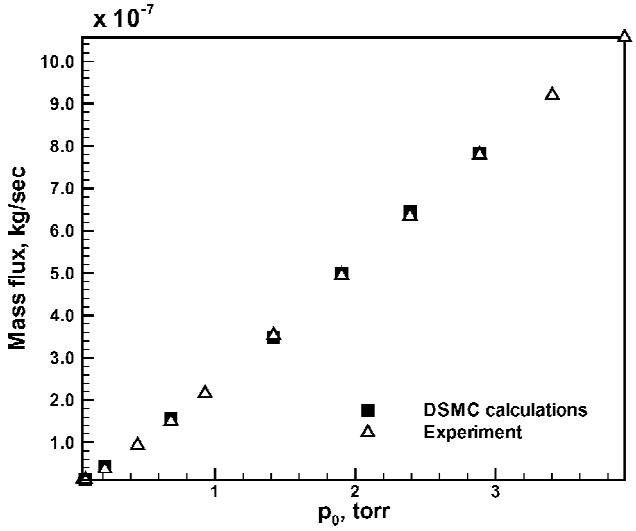

Fig. 11 Mass flux vs plenum pressure for Argon.

not perturb the background gas for the lowest calculated plenum pressures. In this case, the flow is in the free molecular regime in the whole computational domain, and the density of the background gas does not change significantly throughout the field. For higher pressures, the jet significantly modifies the initially uniform background gas density. Figure 12 shows the number density of the background gas normalized by the number density corresponding to a background pressure of 4.2×10^{-4} torr, and for a plenum pressure of 3 torr (case 14, Table 1). Note that the normalized density decreases from its far-field value (taken at about $25d$ downstream from the orifice) to less than 0.05 in the vicinity of the orifice. The jet flow effectively shadows the near field of the orifice, displacing the background molecules from the region close to the outer plenum surface.

The decrease in the density of the background gas is due to collisions between jet and background molecules. Figure 13 shows the molecular mean free path normalized by the orifice diameter and indicates a sufficient collision rate to explain the structure seen in Fig. 12. Generally, the mean free path is comparable or less than the linear size of the plenum height of $30d$. Even at a distance of $20d$ from the orifice, the mean free path is about $50d$, which significantly lowers the penetration of the background molecules upstream to the surface.

The influence of the plenum pressure on the pressure distribution of the background gas along the plenum surface (the line labeled

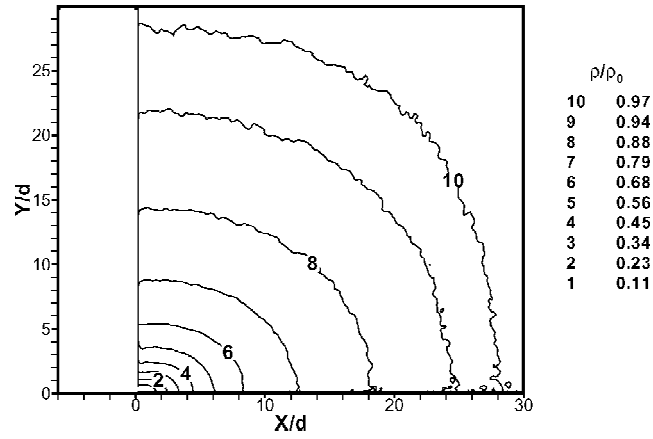

Fig. 12 Normalized density of background gas for case 14.

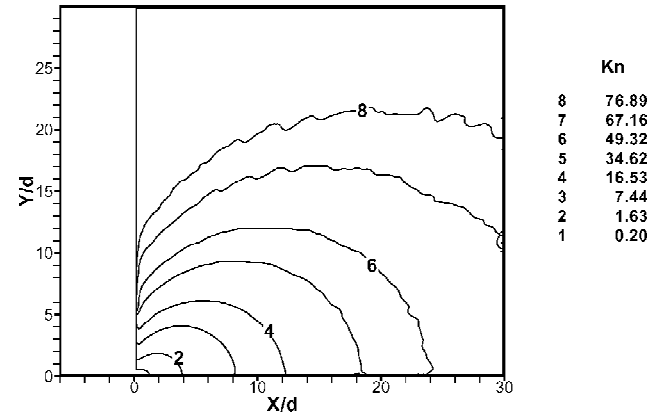

Fig. 13 Local mean free path normalized by the orifice diameter for case 14.

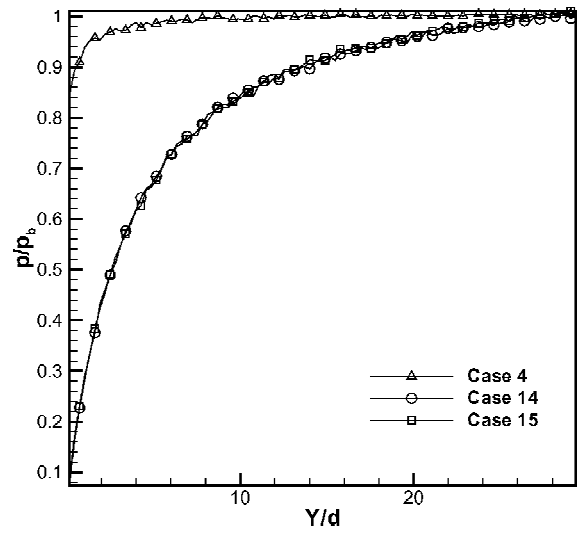

Fig. 14 Normalized pressure distribution of the background gas along the plenum wall.

"wall" in Fig. 3) is shown in Fig. 14. The orifice edge is located at $Y = 0$, and the surface pressure, p_2 of Eq. (10), is normalized by its value at $Y = \infty$, p_b. The surface pressure is almost not affected by the jet for the low-pressure case, $p_0 = 0.1$ torr. It decreases to 0.9 in the vicinity of the orifice edge, being close to unity for $Y > 5d$. For the high-pressure case, the entire area of the plenum is partially shadowed by the flow from the orifice.

The calculations were also performed for other background pressures (cases 12–15 in Table 1). An important conclusion here is that

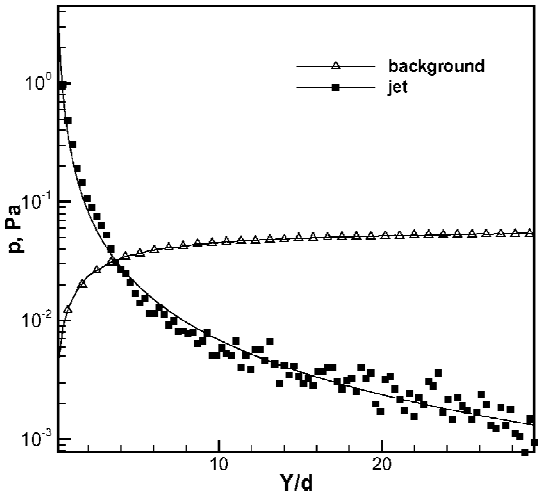

Fig. 15 Pressure distribution along the plenum wall.

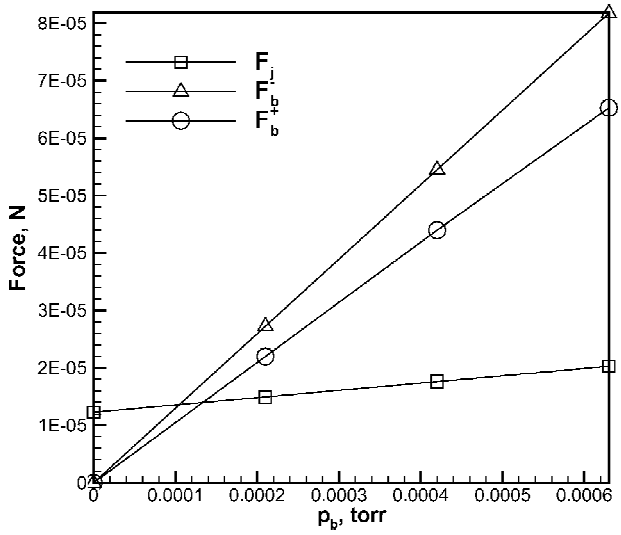

Fig. 16 Different forces as function of the background pressure.

the change in the background pressure from 0 to about 0.02% of the plenum pressure does not impact the penetration of the background gas through the jet to the surface. The shadowing effect is, therefore, the same, and the surface pressure produced by the background gas is similar for different p_b at the same plenum pressure. This is shown in Fig. 14 for two different background pressure values (cases 14 and 15).

To calculate the total force properly, in addition to the thrust force and the forces produced by the background, we need to include the contribution from the force produced by the orifice backflow, that is, molecules from the jet that hit the surface. The comparison of surface pressure distributions due to jet and background gas molecules is given in Fig. 15 for case 14. Note that, in the vicinity of the orifice, the surface pressure produced by jet molecules is much larger than that from the background, whereas the background gas pressure is larger at $Y/d > 5$. From the pressure distributions, F_b^+ and F_j can be calculated by integration over the plenum surface. Because the surface area for the axisymmetric case is proportional, Y^2, the contribution to the force from background pressure F_b^+ turns out to be larger than that of the jet F_j, 4.4×10^{-5} N and 1.76×10^{-5} N, respectively.

The surface pressure from the jet increases with the background pressure, because jet background collisions occur more frequently. This increase is close to linear, as is shown in Fig. 16 for cases 12–15. As was discussed earlier, the surface distribution of the background pressure scales linearly with the background pressure. The force produced by the background gas on the orifice side of the plenum, therefore, also scales linearly (Fig. 16). The influence of the background on the flow from the orifice is negligibly small, which results in a linear dependence of the total force on the background pressure. The computational results, therefore, confirm the applicability of the linear extrapolation from nonzero pressures to obtain thrust measurements for zero background pressure used in Ref. 6. An important conclusion from Fig. 16 is also that the contribution from F_j and F_b^+ is larger than that from F_b^- for all background pressures under consideration.

D. Thrust Stand Calibration

The force has been measured in the experiment by the torsional thrust stand in terms of a deflection sensed by a transducer.[6,7] A calibration of the thrust stand has been carried out by the least square fit of the deflection data and the DSMC simulation results for N_2, He, and Ar. The calibration factor was determined to be 2.2×10^{-3} N/V. Figures 17–19 show the comparison of calculated forces with the calibrated measured force for the three test gases. Because the orifice flow test is easy to set up, and the gases under consideration are readily available, the mass flux and thrust data presented in this paper can be used as a reference for testing micro-Newton thrust stands.

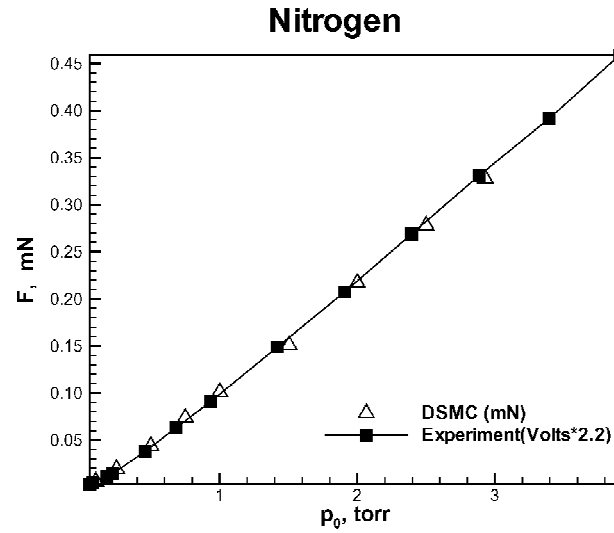

Fig. 17 Measured and calculated total force for nitrogen.

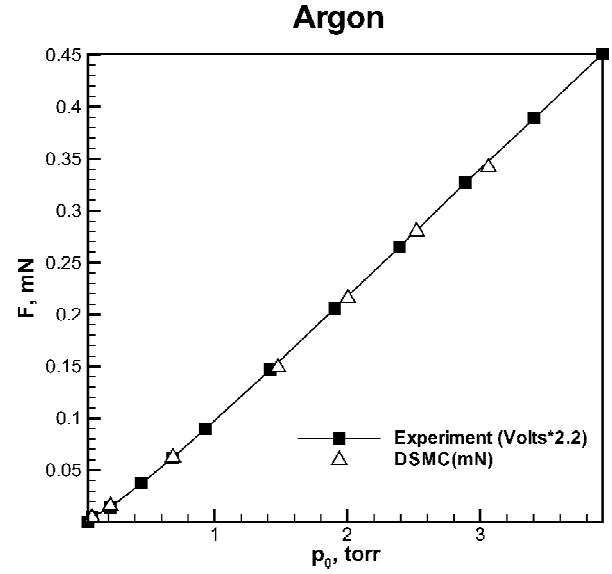

Fig. 18 Measured and calculated total force for argon.

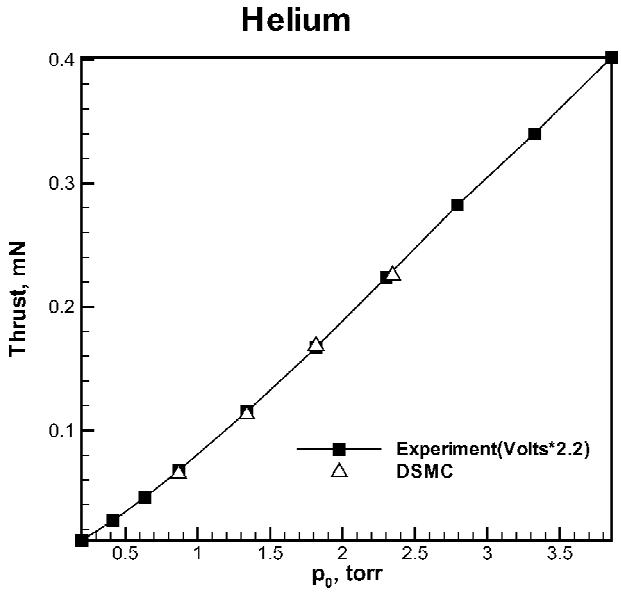

Fig. 19 Measured and calculated total force for helium.

VI. Conclusions

The DSMC method was applied to model a rarefied gas expansion through a thin circular orifice. The calculations were conducted for orifice flow for $Kn = 0.01$–40. The numerical and earlier obtained experimental results were used to calibrate a torsional thrust stand designed to measure force levels from 10^{-6} to 10^{-3} N.

For the nitrogen test gas, the calculated and measured mass flux agree within 5% for Knudsen numbers less than 0.1. The maximum deviation between the calibrated measured and calculated force is 23% for $Kn = 0.4$ and is less than 3% for Kn less than 0.1. For the other two gases, argon and helium, data were obtained for lower background pressures, resulting in even better agreement between measurements and calculations.

The calculations have been made for different facility background pressures, with the background to plenum pressure ratio changed from 0 to 10^{-3}. For low Knudsen numbers, the background gas contribution to the total force becomes significant. This is due to the jet shadowing effect, which is sufficiently significant that it must be included in modeling to permit a comparison with experiment. The increase of the background gas force on the plenum side was found to be a linear function of background pressure.

The force contribution of the momentum flux from the jet on the plenum surface was shown to be important for lower Knudsen numbers. It is comparable to the background gas contribution for $Kn = 0.01$. For the considered flow conditions, the jet backflow contribution linearly increases with background pressure. The total force, therefore, depends linearly on the facility background pressure. Hence, the computational results confirm the applicability of the linear assumption utilized in the experiments to extrapolate the results to a zero background pressure. Moreover, these calculations support the use of ground-based facilities to make reliable low-thrust measurements.

Acknowledgments

The work at the Pennsylvania State University was supported by the U.S. Air Force Office of Scientific Research by Grant F49620-02-1-0104. We would like to thank Clifton C. B. Philips of Space and Naval Warfare Command Systems Center (SPAWARSYSCEN), San Diego who provided us with computer time on the Department of Defense Maui High Performance Computing Center. M. S. Ivanov was supported by NATO Collaborative Linkage Grant SA (PST.CLG 975431) 5066.

References

[1]Scott, J. E., Jr., Morton, H. S., Jr., Phillips, J. A., and Moonan, J. F., "Distribution Function Measurements in Rarefied Gas Flow Through an Orifice," *Proceedings of the 4th International Symposium*, edited by J. H. deLeeuw, Academic Press, New York, Vol. II, 1966.

[2]Liepmann, H. W., "Gaskinetics and Gasdynamics of Orifice Flow," *Journal of Fluid Mechanics*, Vol. 10, 1961, pp. 65–79.

[3]Willis, D. R., Aerospace Engineering. Rept. 440, Princeton Univ., Princeton, NJ, 1960.

[4]Livesey, R., "Flow of Gases Through Tubes and Orifices," *Foundations of Vacuum Science and Technology*, edited by J. M. Lafferty, Wiley-Interscience, New York, 1998, pp. 81–140.

[5]Wadsworth, D. C., and Erwin, D. A., "Translational Nonequilibrium in Rarefied Flow Through a Slit," *Rarefied Gas Dynamics: Experimental Techniques and Physical Systems*, edited by B. D. Shizgal and D. P. Weaver, Vol. 158, Progress in Aeronautics and Astronautics, AIAA, Washington, DC, 1994.

[6]Ketsdever, A. D., Green, A., and Muntz, E. P., "Momentum Flux Measurements from Under Expanded Orifices: Application for Micropropulsion Systems," AIAA Paper 2001-0502, Jan. 2001.

[7]Tew, J., Van Den Driessche, J., Lutfy, F. M., Muntz, E. P., Wong, J., and Ketsdever, A. D., "A Thrust Stand Designed for Performance Measurements of the Free Molecule Micro-Resistojet," AIAA Paper 2000-3673, July 2000.

[8]Ivanov, M. S., Markelov, G. N., and Gimelshein, S. F., "Statistical Simulation of Reactive Rarefied Flows: Numerical Approach and Applications," AIAA Paper 98-2669, June 1998.

[9]Ivanov, M. S., and Rogasinsky, S. V., "Analysis of Numerical Techniques of the Direct Simulation Monte Carlo Method in the Rarefied Gas Dynamics," *Soviet Journal of Numerical Analysis and Mathematical Modeling*, Vol. 2, No. 6, 1988, pp. 453–465.

[10]Bird, G. A., *Monte Carlo Simulations in Engineering Context*, Vol. 74, Progress in Aeronautics and Astronautics, AIAA, New York, 1981, pp. 239–255.

[11]Bird, G. A., *Molecular Gas Dynamics and the Direct Simulation of Gas Flows*, Clarendon, Oxford, England, U.K., 1994.